Spectator Behavior in a Quantum Hall Antidot with Multiple Bound Modes

W.-R. Lee and H.-S. Sim

Department of Physics, Korea Advanced Institute of Science and Technology, Daejeon 305-701, Korea
(Received 24 August 2009; published 12 May 2010)

We theoretically study Aharonov-Bohm resonances in an antidot system with multiple bound modes in the integer quantum Hall regime, taking capacitive interactions between the modes into account. We find the spectator behavior that the resonances of some modes disappear and instead are replaced by those of other modes, due to internal charge relaxation between the modes. This behavior is a possible origin of the features of previous experimental data which remain unexplained, spectator behavior in an antidot molecule and resonances in a single antidot with three modes.

PACS numbers: 73.43.−f, 73.23.Hk

Electron-electron interactions play an important role in an antidot in the integer quantum Hall regime [1]. In an antidot with one or two bound modes (edge states), the number of which is determined by local filling factor ν_c around the antidot, the interactions cause interesting phenomena [2–9], such as charging effects and $h/2e$ Aharonov-Bohm (AB) effects. It is valuable to extend the phenomena to generic effects in antidots with multiple modes. The extension is reminiscent of the stream of studies from a quantum dot to multiple dots [10], and useful for applying antidots to the fractional quantum Hall regime [11,12] or to qubit implementation [13].

Some works [14–16] have been done in that direction, but require further studies. In Ref. [14], an antidot molecule with $\nu_c = 4$ was experimentally studied; see a simplified view with $\nu_c = 2$ in Fig. 1(a). It has atomic modes X_1, X_2, and molecular modes Y. Under certain conditions, AB resonances with period ΔB_Y corresponding to the area enclosed by Y disappear in electron conductance G_T through the system, while those to $X_{1,2}$ were observed [Fig. 1(c)]. This finding disagrees with the noninteracting electron case, in which Y more clearly shows AB resonances than $X_{1,2}$ since Y couples more strongly with extended edge channels. Such disappearance of AB resonances was called spectator behavior [14]. Its mechanism remains unclear despite of efforts [17].

Unexpected experimental results [15] were also found in a $\nu_c = 3$ antidot with three modes [Fig. 1(b)]. The magnetic-field dependence of G_T shows three peaks in one AB period ΔB, two of which have almost same peak height higher than the third [Fig. 1(d)]. And, the dependence of G_T on the backgate voltage V_{BG} applied to the antidot shows two alternating peak separations, i.e., the pairing of two neighboring peaks. Even more strange is that the peak pairing was not found for $\nu_c = 2$ and 4. These features disagree with the noninteracting case, in which there appear three independent peaks with different height and separation within one period since each mode shows one peak per period and couples to extended edge channels differently from the others; for example, X_1 couples to channels $1\uparrow$ and $2'\uparrow$, while X_2 to $0\downarrow$ and $1'\downarrow$ [Fig. 1(b)].

The unexpected results may come from the interactions; however, they are different from the $h/3e$ AB effect, a naive extension of the $h/2e$ AB effect [2] of $\nu_c = 2$, in which the three peaks have the same height.

In this Letter, we theoretically study AB resonances in antidot systems with three modes in the integer quantum Hall regime, based on a capacitive interaction model. We predict the *spectator* behavior that the AB resonances of some modes disappear and instead are replaced by those of other modes because of internal charge relaxation between the modes. Which and how many modes show the spectator behavior depends on ratios of capacitances. Our finding provides unified understanding of the unexpected results [14,15] on the two different systems.

Antidots with three modes.—We consider two representative systems with three modes, a symmetric $\nu_c = 2$
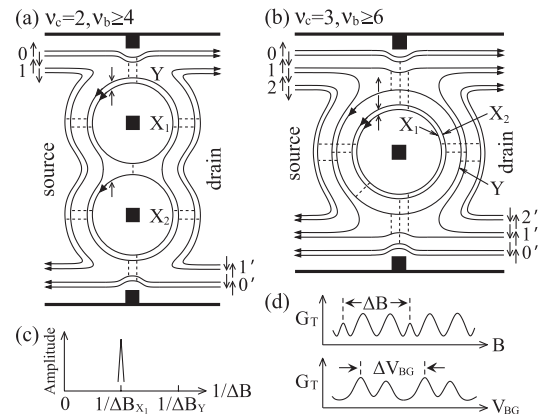

FIG. 1. Schematic views of (a–b) antidots and (c–d) relevant experimental data. (a) A symmetric antidot molecule with local filling factor $\nu_c = 2$ and bulk filling $\nu_b \geq 4$. It has atomic modes X_1, X_2, and molecular mode Y. Each mode has Landau-level (0, 1, 2) and spin ($\uparrow$, $\downarrow$) indexes. The solid and dashed lines represent edge states and electron tunneling, respectively. (b) A $\nu_c = 3$ antidot with modes X_1, X_2, Y. (c) Fourier transformation of AB oscillations of conductance G_T through an antidot molecule with $\nu_c = 4$. From [14]. (d) Magnetic-field B and backgate-voltage V_{BG} dependence of G_T for an antidot with $\nu_c = 3$. From Figs. 11 and 13 of [15].

molecule and a $\nu_c = 3$ antidot [15] (Fig. 1); a $\nu_c = 4$ molecule in Ref. [14] is spin-unresolved so that some of its features can be described by the $\nu_c = 2$ molecule. Each mode tunnel couples to extended edge channels with the same spin, and also to the other modes with the same spin. The two systems have one outermost mode Y and two inner modes X_1 and X_2. We treat X_1 and X_2 equally, since in the molecule they are symmetric, and in the $\nu_c = 3$ antidot, they have Zeeman gap (albeit exchange enhanced [18]) much smaller than Landau gap.

We consider the regime of zero bias, zero temperature, and strong perpendicular magnetic field $B_0 \gg \Delta B_\alpha$. Here, ΔB_α is the AB period of mode $\alpha = X_1, X_2, Y$. In the tunneling regime, we describe the total energy of the two systems by the same form (with system-dependent parameters) of the capacitive interaction model,

$$E(\{\delta Q_\alpha\}) = \sum_{\alpha m} \tilde{\xi}_{\alpha m} n_{\alpha m} + \sum_{\alpha \alpha'} U_{\alpha \alpha'} \delta Q_\alpha \delta Q_{\alpha'} / e^2, \quad (1)$$

where $\alpha, \alpha' = X_1, X_2, Y$. We derive it by generalizing the case of a $\nu_c = 2$ antidot [1,7] in the same way as in multiple dots [10]. It governs the ground-state transition as a function of B_0 or V_{BG}. By analyzing the transition, we predict the features (height and separation) of AB resonance peaks in G_T. For the $\nu_c = 2$ case, the model (1) successfully describes the charging effect, $h/(2e)$ AB effect and Kondo effect [7]; we here ignore Kondo effects.

The first term of Eq. (1) comes from the energy $\tilde{\xi}_{\alpha m}$ and occupation $n_{\alpha m}$ of single-electron orbital m of α. We will derive below that $\tilde{\xi}$ satisfies $\tilde{\xi}_{\alpha m} = \xi_{\alpha m, 0} + \Delta \xi_\alpha \delta B / \Delta B_\alpha$ when the magnetic field varies from B_0 by $\delta B (\ll B_0)$. Here, $\Delta \xi_\alpha$ is the single-particle level spacing of α, and $\tilde{\xi}_{\alpha m} = \xi_{\alpha m, 0}$ at B_0. This dependence of $\tilde{\xi}_{\alpha m}$ on δB leads to the fact that mode α shows one AB resonance per period ΔB_α in the noninteracting limit.

The second term of Eq. (1) shows capacitive interactions $U_{\alpha \alpha'} \equiv e^2 (C^{-1})_{\alpha \alpha'} / 2$ between the excess charges δQ_α accumulated in mode α. δQ_α depends on δB as

$$\delta Q_\alpha = eN_\alpha - Q_\alpha^G + e \delta B / \Delta B_\alpha. \quad (2)$$

The total charge eN_α of α is compensated by gate charge Q_α^G ($\propto V_{BG}$) tuned by V_{BG}. $N_\alpha (= \sum_m n_{\alpha m})$ varies by an integer due to the discreteness of electron charge $e < 0$.

We explain the dependence of $\tilde{\xi}_{\alpha m}$ and δQ_α on δB. As B_0 increases by δB, each orbital αm spatially shifts toward the center of its antidot to keep enclosing a given number, saying m, of magnetic flux quanta. Then, its energy changes by $(\Delta \xi_\alpha + 2\sum_{\alpha'} U_{\alpha' \alpha} \delta Q_{\alpha'} / eN_\alpha) \delta B / \Delta B_\alpha$. The term $\Delta \xi_\alpha \delta B / \Delta B_\alpha$, coming from antidot potential, results in the dependence of $\tilde{\xi}_{\alpha m}$ on δB. The other term, resulting from the interactions between the orbital and $\delta Q_{\alpha'}$, causes the dependence on δB in Eq. (2). The dependence on δB captures the physics of antidots.

We discuss the parameters of Eq. (1). For $B_0 \gg \Delta B_\alpha$, it is natural to apply the constant interaction model [10] that $\Delta \xi_\alpha$ and $C_{\alpha \alpha'}$ are constant over several AB periods, and

that $C_{\alpha \alpha} = |C_{g,\alpha}| + \sum_{\alpha' \neq \alpha} |C_{\alpha \alpha'}|$. $C_{g,\alpha}$ is the "gate" capacitance of α due to extended edge channels and V_{BG}. X_1 and X_2 have the same values of ΔB_α, $\Delta \xi_\alpha$, $U_{\alpha \alpha}$, $U_{\alpha Y}$, and $C_{g,\alpha}$ because of the symmetry.

Charge accumulation and relaxation.—As δB increases, δQ_α continuously accumulates with rate $1/\Delta B_\alpha$ as in Eq. (2). The accumulated charges are relaxed with resonant tunneling, resulting in the transition of the ground-state configuration (N_{X_1}, N_{X_2}, N_Y). There are two kinds of single-electron relaxation. External relaxation occurs between a mode (here, X_1) and extended edge channels (with Fermi level ϵ_F), e.g., when $E(\delta Q_{X_1} \pm e, \delta Q_{X_2}, \delta Q_Y) = E(\delta Q_{X_1}, \delta Q_{X_2}, \delta Q_Y) \pm \epsilon_F$. This causes resonance peaks in G_T. By contrast, *internal* relaxation occurs between modes, through tunneling or cotunneling mediated by virtual states, e.g., when

$$E(\delta Q_{X_1} \pm e, \delta Q_{X_2}, \delta Q_Y \mp e) = E(\delta Q_{X_1}, \delta Q_{X_2}, \delta Q_Y). \quad (3)$$

It does not cause peaks in G_T. It occurs only between Y and $\alpha \in \{X_1, X_2\}$ in our case with the symmetry between X_1 and X_2. In general, relaxations involving more than one electron can occur. Two-electron relaxation occurs in the molecule (see below), while not in the $\nu_c = 3$ antidot.

The ground-state evolution of the antidots and the resulting AB resonances are governed by the relaxations. We study them by analyzing a charge stability diagram [10]. In Fig. 2(a), it is drawn for a $\nu_c = 3$ antidot in $(\delta Q_{X_+}, \delta Q_Y)$ plane, where $\delta Q_{X_\pm} \equiv \delta Q_{X_1} \pm \delta Q_{X_2}$; this two-dimensional view is possible due to the symmetry of X_1 and X_2. Below, we first consider the strong interaction regime of $U_{\alpha \alpha} \gg \Delta \xi_\alpha$, which is analogous to the case of metallic dots, and then discuss finite $\Delta \xi_\alpha$.

The internal relaxation results in the spectator behavior. The evolution of $\{\delta Q_\alpha\}$ follows different types of sequences of AB resonances, depending on how many times the spectator behavior appears per ΔB_{X_1}. For example, in a $\nu_c = 3$ antidot, there are three types I, II, III [Fig. 2]. In type I of X_1-Y-X_2, the evolution never passes the internal relaxation, and AB resonances occur sequentially by X_1, Y, X_2, X_1, Y, X_2, $\cdots$. In type II of X_1-Y-Y (III of Y-Y-Y), the evolution passes the internal relaxation once (twice) per ΔB_{X_1}, and the AB resonances by X_2 (X_1 and X_2) disappear and are replaced by those by Y. Here, X_1 or X_2 shows the spectator behavior.

We discuss the general features of the spectator behavior. Which mode shows the behavior is governed by

$$\eta \equiv \frac{(U_{X_1 X_1} + U_{X_1 X_2} - 2U_{X_1 Y}) \delta B / \Delta B_{X_1}}{(U_{YY} - U_{X_1 Y}) \delta B / \Delta B_Y} = \frac{C_{g,Y} \Delta B_Y}{C_{g,X_1} \Delta B_{X_1}}, \quad (4)$$

the ratio of energy gains between δQ_{X_+} ($= \delta Q_{X_1} + \delta Q_{X_2}$), and δQ_Y in the internal relaxation between them; see Eq. (3). In Fig. 2(a), η equals the ratio of slopes between the dash-dot relaxation line and the evolution arrow. When
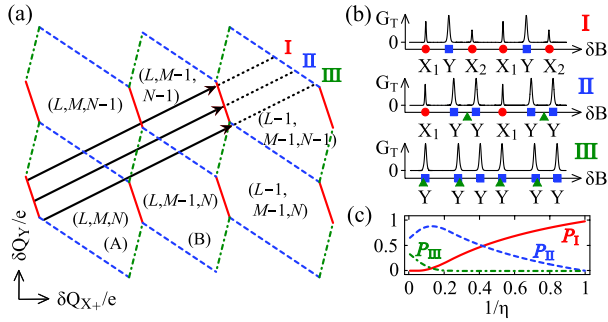
FIG. 2 (color online). (a) Charge stability diagram for a $\nu_c = 3$ antidot. It consists of two types (A) and (B) of hexagonal cells in $(\delta Q_{X_+}, \delta Q_Y)$ plane. Each cell represents a ground-state configuration of $(N_{X_1}, N_{X_2}, N_Y) = (L, M, N)$. Cell boundaries are determined by charge relaxation conditions such as Eq. (3). At dashed blue (solid red) boundaries, AB resonances occur via tunneling through Y (X_1 or X_2), and at dash-dot green boundaries internal charge relaxations occur between Y and $X_{1,2}$. As the magnetic field increases, $(\delta Q_{X_+}, \delta Q_Y)$ evolve along a line (solid arrow) of slope $\Delta B_{X_1}/(2\Delta B_Y)$, while δQ_{X_-} is constant within a cell and differs by charge e between (A) and (B). Depending on initial values of δQ_α's at given field B_0, the evolution shows one of three possible sequences of AB resonances, "X_1-Y-X_2" (type I), "X_1-Y-Y" (type II), "Y-Y-Y" (type III). Parameters are chosen as $\Delta \xi_\alpha = 0$, $\Delta B_{X_1} = \Delta B_Y$, $C_{g,Y} = 8 C_{g,X_1}$, $C_{X_1Y} = 2 C_{g,X_1}$, $C_{X_1X_2} = 8 C_{X_1Y}$, and $\delta Q_{X_-} = 0$ for cell (A) and $-e$ for (B). (b) Sequence of resonance peaks in G_T as a function of δB for each type shown in (a). The modes giving peaks are shown. Triangles represent internal charge relaxation. (c) Probability $P_J(1/\eta)$ of finding the sequences of type $J = $ I, II, III is drawn with the parameters of (a).

$\eta < 1$, the relaxation occurs from δQ_Y to δQ_{X_1} or δQ_{X_2}; hence, Y shows the spectator behavior. For $\eta > 1$, X_1 and X_2 show it. On the other hand, the intermode interaction strength ($\propto |C_{\alpha'\alpha(\neq\alpha')}|$) also governs the behavior. As the strength increases and as η more and more deviates from 1, more sequences (with different "initial" values of $\{\delta Q_\alpha\}$ at B_0) show the behavior (type II or III); the dash-dot line in Fig. 2(a) becomes longer so that the evolution has more chance to pass the internal relaxation. When the strength vanishes or $\eta = 1$, the spectator behavior is suppressed and only type I appears. Note that noninteracting electrons show only type I.

Antidot with $\nu_c = 3$.—We discuss the spectator behavior in a $\nu_c = 3$ antidot [Fig. 1(b)]. Its geometry indicates $\Delta B_{X_1} \simeq \Delta B_Y$ and $|C_{X_1X_2}| > |C_{X_1Y}|$. The spatial separation between the outermost mode Y (inner modes $X_{1,2}$) and the extended channels $1\downarrow$ is governed by Zeeman splitting energy (Landau gap) so that $C_{g,Y}/C_{g,X_1}$ is much larger than 1. These lead to $\eta > 1$ [Eq. (4)]. Hence, as mentioned above, X_1 and X_2 show the spectator behavior that type II sequence of X_1-Y-Y and III of Y-Y-Y appear instead of I of X_1-Y-X_2. As η (> 1) and $|C_{X_{1,2}Y}|$ increase, type II and III appear more dominantly. For a $\nu_c = 3$ antidot, we obtain the probability $P_J(1/\eta)$ of finding type $J \in \{$I, II, III$\}$ in the

ensemble of sequences with different initial values of $\{\delta Q_\alpha\}$ at B_0 [Fig. 2(c)].

In Fig. 2(b), we plot $G_T(\delta B)$. We obtain it in the sequential tunneling regime using the standard master equation method [16], which is enough for demonstrating the positions and relative heights of AB peaks; here, we assumed low temperature ($\ll U_{\alpha\alpha}$) and the backward-reflection regime, as in Ref. [15], that mode α couples to edge channel β with coupling strength $\gamma_{\alpha\text{-}\beta}$ as $\gamma_{Y-1\uparrow} > \gamma_{X_1-1\uparrow} > \cdots$. For each type, we describe the features of G_T. In type I, each of X_1, X_2, and Y shows one peak per period ΔB_{X_1}. The resulting three peaks in ΔB_{X_1} have different height because of different $\gamma_{\alpha\text{-}\beta}$'s. The peak by Y is the highest since Y is the outermost mode.

In type II, two peaks among the three within ΔB_{X_1} come from Y and have the same height higher than the third. The separation $\kappa \Delta B_{X_1}$ between two consecutive peaks by Y depends on interactions as $\kappa = U_{X_1Y}/(2U_{X_1Y} + U_{YY})$, regardless of the initial values of $\{\delta Q_\alpha\}$ at B_0. In the strong intermode interaction limit of $C_{g,X_1}/C_{X_1Y} \to 0$, $\kappa \to 1/3$. The position of the other peak by X_1 or X_2 depends on the initial values of $\{\delta Q_\alpha\}$.

In type III, all the three peaks within ΔB_{X_1} come from Y, showing the same peaks. The separation between them is determined by interactions as $\kappa \Delta B_{X_1}$ and $(1 - 2\kappa)\Delta B_{X_1}$. In the strong intermode interaction limit, it becomes $\Delta B_{X_1}/3$, showing $h/(3e)$ AB effects, and the total energy in Eq. (1) becomes $E \simeq U\delta Q_{\text{tot}}^2/e^2$, where $\delta Q_{\text{tot}} = \sum_\alpha \delta Q_\alpha = 3e\delta B/\Delta B_{X_1} + \cdots$. This form of E, mentioned in literatures [16], cannot describe type II.

So far, we have restricted to $\Delta \xi_\alpha = 0$. In the case of finite level spacing $\Delta \xi_\alpha$, the first term of Eq. (1) is absorbed into the second so that E has the same form as that of $\Delta \xi_\alpha = 0$, but with replacement (i) $U_{\alpha\alpha} \to U_{\alpha\alpha} + \Delta \xi_\alpha/2$ and (ii) $Q_\alpha^G \to \tilde{Q}_\alpha^G$, where $\tilde{Q}_\alpha^G$ is obtained by $\sum_{\alpha'}(U_{\alpha\alpha'} + \delta_{\alpha\alpha'}\Delta \xi_\alpha/2)\tilde{Q}_{\alpha'}^G = \sum_{\alpha'} U_{\alpha\alpha'}Q_{\alpha'}^G$. The replacement does not modify the dependence of δQ_α on δB in Eq. (2), but weakens the spectator behavior [see replacement (i)]. For example, when $\Delta \xi_\alpha$ is comparable to $e^2/C_{X_1X_1}$, type II and III are suppressed by 25% and 100%, respectively, for the antidot studied in Fig. 2.

The above findings indicate that the result of Ref. [15], two peaks with equal height in ΔB [the upper panel of Fig. 1(d)], may be explained by type II; we do not exclude the possibility of type I that two modes among the three accidently give the two peaks with almost equal height.

On the other hand, replacement (ii) affects the evolution of δQ_α as a function of V_{BG}. For $\Delta \xi_\alpha = 0$, the evolution follows a line of slope $Q_Y^G/(2Q_{X_1}^G) \simeq 0.5$ in the stability diagram. When $\Delta \xi_\alpha$ is finite, the slope becomes $s = \tilde{Q}_Y^G/(2\tilde{Q}_{X_1}^G) \simeq 0.5[1 + (|C_{g,X_1}| + 3|C_{X_1Y}|)\Delta \xi_{X_1}/e^2]/[1 + (|C_{g,Y}| + 3|C_{X_1Y}|)\Delta \xi_Y/e^2]$. s can be very small for $\Delta \xi_\alpha \simeq e^2/|C_{X_1Y}|$, $|C_{g,Y}| \gg |C_{g,X_1}|$, $|C_{X_1Y}|$. The latter condition can be satisfied in a $\nu_c = 3$ antidot since the spatial separation between Y (X_1) and extended edge channels is
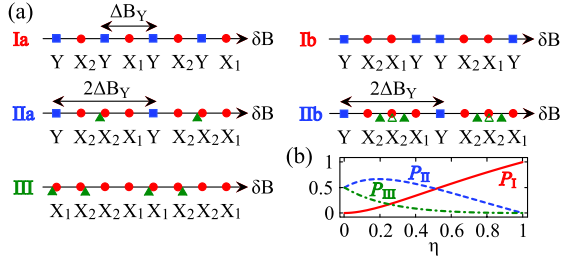
FIG. 3 (color online). (a) Selected types of sequences of AB resonances, as a function of δB for a $\nu_c = 2$ molecule. Filled and empty triangles represent the single- and two-electron internal relaxations, respectively. (b) Probability $P_J(\eta)$ of finding the sequences of type $J = $ I, II, III. Here, I (II) means the types, e.g., Ia and Ib (IIa and IIb), having two (one) Y resonances within ΔB_{X_1}. Parameters are chosen as $\Delta \xi_\alpha = 0$, $\Delta B_{X_1} = 2\Delta B_Y$, $C_{X_1Y} = 10 C_{g,X_1}$, and $C_{X_1X_2} = 0.5 C_{X_1Y}$.

determined by Zeeman (Landau) splitting. The evolution line with small slope s can pass only the solid boundaries in the stability diagram [Fig. 2], showing paired peaks by X_1 and X_2. Or, depending on the initial value of $\{Q_\alpha\}$ at B_0, it can pass only the dashed lines, showing paired peaks by Y. The paired peaks agree with the lower panel of Fig. 1(d). In the cases of $\nu_c = 2$ and 4 with finite $\Delta \xi_\alpha$, the slope s has a similar form to $\nu_c = 3$, but the peak pairing does not appear because the separation between the outermost mode and edge channels is governed by Landau splitting so that s has a similar value to the case of $\Delta \xi_\alpha = 0$. These indicate that the peak pairing in Ref. [15] is due to finite $\Delta \xi_\alpha$ and the interaction between Y and edge channels.

Molecule.—We discuss the molecule in Fig. 1(a). Its geometry implies $\Delta B_{X_1} \gtrsim 2\Delta B_Y$ and $|C_{X_1X_2}| < |C_{X_1Y}|$. Since the circumference of Y is shorter than 2 times of that of X_1, one has $|C_{g,Y}| < 2|C_{g,X_1}|$, provided that V_{BG} affects $C_{g,Y}$ and C_{g,X_1} more dominantly than edge channels. Then, $\eta < 1$, and Y shows the spectator behavior.

For an example case of $C_{X_1X_2} = 0.5 C_{X_1Y}$, selected AB resonance sequences are shown as a function of δB in Fig. 3. The spectator behavior occurs such that type Ia of Y-X_2-Y-X_1 is replaced by IIa of Y-X_2-X_2-X_1 (III of X_1-X_2-X_2-X_1) when the relaxation in Eq. (3) occurs once (twice) within ΔB_{X_1}. In the molecule, in addition to the one-electron relaxation, there occurs two-electron relaxation, $E(\delta Q_{X_1} \pm e, \delta Q_{X_2} \pm e, \delta Q_Y \mp e) = E(\delta Q_{X_1}, \delta Q_{X_2}, \delta Q_Y) \pm \epsilon_F$, which is a mixture of internal and external relaxations. This additional process results in more types such as IIb of Y-X_2-X_2-X_1. Type IIb has the same sequence as IIa, and results from Ib of Y-X_2-X_1-Y due to two one-electron internal relaxations and one two-electron relaxation within ΔB_{X_1}. We plot $P_J(\eta)$ of type J in Fig. 3(b). As η decreases from 1, type II (e.g., IIa and IIb) becomes dominant. Note that when $\Delta \xi_\alpha \simeq e^2/C_{\alpha\alpha}$, P_{II} and P_{III} are reduced by less than 10% for $0.6 \lesssim \eta < 1$. Qualitatively same features appear in other parameter ranges.

The unexpected results of Ref. [14] can be understood by type II, provided that the inner modes X_1 and X_2 are almost decoupled from edge channels (i.e., only Y shows AB peaks). In this case, the period of AB peaks in type II is $2\Delta B_Y$ instead of ΔB_Y due to the spectator behavior [Fig. 3(a)]. This agrees with Fig. 1(c), since $2\Delta B_Y \simeq \Delta B_{X_1}$. On the contrary, all the other types of $\eta < 1$ and those of $\eta > 1$ cannot explain Fig. 1(c); for example, type I shows peaks with ΔB_Y or a mixture of ΔB_Y and ΔB_{X_1}, depending on the coupling of $X_{1,2}$ with edge channels. These indicate that the molecule of Ref. [14] is in the regime of type II of $\eta < 1$.

Conclusion.—Electron-electron interactions give rise to the spectator behavior of AB resonances in antidots with three modes. The spectator behavior is generic, i.e., expected to appear in other quantum Hall systems with multiple modes, such as antidots and quantum dots. And it is useful for detecting interactions between edge states. To experimentally test the spectator behavior and our explanation of the experimental data [14,15], one can monitor the modes showing resonance signals by selective injection and detection of edge channels [19].

[1] H.-S. Sim, M. Kataoka, and C. J. B. Ford, Phys. Rep. **456**, 127 (2008).
[2] C. J. B. Ford *et al.*, Phys. Rev. B **49**, 17456 (1994); M. Kataoka *et al.*, Phys. Rev. B **62**, R4817 (2000).
[3] I. J. Maasilta and V. J. Goldman, Phys. Rev. B **57**, R4273 (1998).
[4] M. Kataoka *et al.*, Phys. Rev. Lett. **83**, 160 (1999).
[5] I. Karakurt *et al.*, Phys. Rev. Lett. **87**, 146801 (2001).
[6] M. Kataoka, C. J. B. Ford, M. Y. Simmons, and D. A. Ritchie, Phys. Rev. Lett. **89**, 226803 (2002).
[7] H.-S. Sim *et al.*, Phys. Rev. Lett. **91**, 266801 (2003); N. Y. Hwang, S.-R. E. Yang, H.-S. Sim, and H. Yi, Phys. Rev. B **70**, 085322 (2004).
[8] S. Ihnatsenka and I. V. Zozoulenko, Phys. Rev. B **74**, 201303(R) (2006).
[9] M. Kato *et al.*, Phys. Rev. Lett. **102**, 086802 (2009).
[10] W. G. van der Wiel *et al.*, Rev. Mod. Phys. **75**, 1 (2002).
[11] I. J. Maasilta and V. J. Goldman, Phys. Rev. Lett. **84**, 1776 (2000).
[12] D. V. Averin and J. A. Nesteroff, Phys. Rev. Lett. **99**, 096801 (2007).
[13] D. V. Averin and V. J. Goldman, Solid State Commun. **121**, 25 (2001).
[14] C. Gould *et al.*, Phys. Rev. Lett. **77**, 5272 (1996).
[15] V. J. Goldman, J. Liu, and A. Zaslavsky, Phys. Rev. B **77**, 115328 (2008).
[16] S. Ihnatsenka, I. V. Zozoulenko, and G. Kirczenow, Phys. Rev. B **80**, 115303 (2009).
[17] Y. Takagaki, Phys. Rev. B **55**, R16021 (1997).
[18] W. Xu *et al.*, J. Phys. Condens. Matter **7**, 4419 (1995).
[19] M. Kataoka, C. J. B. Ford, M. Y. Simmons, and D. A. Ritchie, Phys. Rev. B **68**, 153305 (2003).